Ultrafast laser damaging of ball bearings for the condition monitoring of a fleet of linear motors

Abdul Jabbar[1], Manuel Mazzonetto[1], Leonardo Orazi[1, 2] and Marco Cocconcelli[1]

[1] *DISMI - University of Modena and Reggio Emilia, Via Amendola 2, Reggio Emilia, 42122, Italy*

[2] *EN&TECH - University of Modena and Reggio Emilia, Piazzale Europa, 1, Reggio Emilia 42124, Italy*
abdul.jabbar@unimore.it
manuel.mazzonetto@unimore.it
leonardo.orazi@unimore.it
marco.cocconcelli@unimore.it

ABSTRACT

Machine learning-based condition monitoring of mechanical systems, such as bearings, employs two primary approaches: unsupervised and supervised methods. Unsupervised approaches aim to characterize the healthy state of the machine and monitor deviations from this state. The advantage lies in requiring only the health condition of the component without the need for historical data until breakdown. However, the disadvantage is the lack of information regarding the root cause of any potential malfunction. On the other hand, supervised methods consider both healthy and faulty cases, aiming to maximize the difference between them through post-processing, as well as among different fault types. The advantage is the ability to analyze the specific signature of a particular fault type. Nonetheless, the disadvantage is that available data usually do not cover all possible faults that may occur. Typically, obtaining a faulty bearing involves either a time-consuming run-to-failure test or the artificial induction of faults using drills, electro-discharge pens, etc. While artificial faults offer a quicker procedure, they often fail to replicate real faults faithfully. This paper suggests using picosecond laser technology to engrave the surface of the bearing and create artificial faults. Modern laser technology allows for precise control over the dimensions of injected faults, enhancing the understanding of fault progression at various stages in the life of bearings. These measurements are crucial parameters for evaluating the robustness of diagnostic algorithms. This paper focuses on artificially damaging a ball bearing used in an independent cart systems application, which comprises a fleet of linear motors moving on the same rail. These systems have recently been proposed by different manufacturers and adopted in the field of packaging machines for their flexibility. For such systems, no prior instances of faulted bearings are available, and the size of a real fault is also unknown. Hand-made faults with drills did not produce discernible faults appreciable in post-processing of the data. Therefore, a picosecond laser with a pulse duration of 10 ps and a maximum energy per pulse of approximately 100 μJ is utilized to create a set of test bearings with increasing fault sizes on the outer race. Post-processing of the data enables the qualification of the minimum fault severity detectable in this specific application.

1. INTRODUCTION

The emerging technology of independent cart systems comprises a fleet of linear motors that operate on a shared track and can be controlled individually and independently. Unlike conventional motors, where the stator and rotor are enclosed within the same frame, linear motors feature a completely detached rotor. In this design, the fixed frame of the motor serves as the stator, with coils evenly distributed along the track, while the single cart functions as the movable part, containing permanent magnets positioned above the coils, along with a set of bearings. The cart, while crucial, is a completely passive component of the system. It interact with the changing magnetic field of the motor coils, moving in synchronization with the magnetic field pattern.

Independent cart systems stand poised to revolutionize traditional conveyor belts. Offering a range of benefits such as increased flexibility and dynamic capabilities, independent cart systems are proving to be ideal solutions for a wide range of industrial and motion control applications. Comprising modular components such as linear motors, guide rails, and control circuitry, these systems offer adaptability and efficiency. Linear motors within independent cart systems are

available in both straight and curved modules, allowing for diverse path configurations tailored to specific industrial requirements. Across industries, various iterations of independent cart systems are being deployed, each with distinct features in guide rail and cart design. Depending on application needs, guide rails may either attach directly to linear motors (Jabbar, D'Elia, & Cocconcelli, 2023; Jabbar, Cocconcelli, D'Elia, & Strozzi, 2023) or form a separate bed parallel to them (see figure 2), a brief description of such a system with parallel guide rail can also be found in (Cavalaglio Camargo Molano, Capelli, Rubini, Borghi, & Cocconcelli, 1968). Similarly, cart and bearings can take on different configurations to suit specific application requirements. For example, in a previous study (Jabbar, D'Elia, & Cocconcelli, 2023; Jabbar, Cocconcelli, et al., 2023), the authors have described setups where guide rails are directly attached to linear motors, with options for 12 or 6 bearings featuring plastic outer races. One significant advantage of independent cart systems is their ability to define the entire track in stations, enabling the accommodation of distinct speed profiles for each cart along every station.

Despite the considerable benefits that these systems offer over conventional conveyors, economic concerns remain. To date, the high cost and substantial upfront investment required for independent cart systems present challenges to their widespread adoption. To ensure economic viability, it is imperative that these systems operate flawlessly. Thus, the implementation of robust condition monitoring measures is crucial for their sustained performance. Although independent cart systems are rapidly replacing conveyor belt systems, there has been a lack of studies focused condition monitoring of such systems. Due to the confidentiality surrounding these systems, often protected by non-disclosure agreements, there is no repository or public database where vibration, acoustic, or other data related to independent cart systems is available for conducting condition monitoring. Consequently, to the best of the authors' knowledge, there has been no research conducted on condition monitoring of the independent cart systems. This scarcity of research and data necessary for condition monitoring serves as a primary motivation for this study. Furthermore, another motivation for this research stems from the inherent challenges associated with monitoring the condition of such systems.

Condition monitoring of the independent cart systems presents a formidable challenge for several reasons. Firstly, it is a highly non-synchronous system, with speed variations ranging from a few millimeters per second to several meters per second. For instance, the system under study can achieve cart's speed of up to 4 meters per second. Additionally, the system supports speed reversal, allowing for changes in direction. Furthermore, with the addition of every cart to the fleet, the number of bearings increases by three. Given that each cart contains three bearings and there are hundreds of bearings in the fleet, monitoring the condition of the independent cart systems becomes complex. This monitoring process can be divided into several steps: firstly, identifying if there is a fault; secondly, determining the type of fault (such as inner race, outer race, ball fault, etc.); thirdly, distinguishing whether the top bearing is faulty or the bottom one; and fourthly, localizing the cart carrying the faulty bearing. Understanding the behavior of the vibration signal in the case of a top bearing fault is also intriguing. This is because there is a pair of bearings with exactly the same dimensions and dynamics supporting the same movement.

There are several bearing datasets available, including the Intelligent Maintenance Systems (IMS) dataset (Lee, Qiu, Yu, & Lin, 2007), the Case Western Reserve University (CWRU) dataset (*Bearing Data Center, Case Western Reserve University (CWRU)*, n.d.), and the IEEE Dataport bearing dataset (B. Hu, 2023). These datasets serve as benchmarks for testing and evaluating new condition monitoring algorithms. However, these datasets primarily focus on conventional configurations where the bearings are fixed around a shaft. In contrast, in independent cart systems, the bearings not only rotate but also translate along the path defined by a set of linear motors. This introduces a significant departure from conventional setups. Additionally, the linear motion of the cart is often highly non-synchronous, resulting in non-synchronous rotational speeds of the bearings. Furthermore, the possibility of instant speed reversal further complicates the dynamics of the system. Given these differences, there is a clear need for new datasets specifically tailored for the condition monitoring of such industrial systems. These datasets would need to capture the unique characteristics and challenges posed by the operation of bearings within independent cart systems.

Data-driven modeling has emerged as a valuable approach that can complement traditional signal processing techniques, offering a robust methodology for uncovering insights from complex datasets. This methodology involves leveraging machine learning algorithms to discern patterns and anomalies within the data. While implementation requires expertise in both data preprocessing and machine learning, the benefits of this approach can be significant. In light of these advantages, researchers have explored the integration of machine learning algorithms for bearing fault classification, alongside classical signal processing techniques. A diverse array of algorithms has been deployed for this purpose, encompassing Long Short Term Memory (LSTM)((Walther & Fuerst, 2022), (Y. Hu et al., 2022)), Autoencoders ((K. Cheng RC.and Chen, 2022), (R.-C. Cheng, Chen, Liu, Chang, & Tsai, 2021)), Support Vector Machines (SVM) ((Sun & Liu, 2023), (Y. Fan, Zhang, Xue, Wang, & Gu, 2020)), Artificial Neural Networks (ANN), Convolutional Neural Networks (CNN), Deep Learning (DL), Transfer Learning (Wan et al., 2022), Anomaly Detection (Z. Fan et al., 2023), and the K-means clustering algorithm (Yiakopoulos, Gryllias, & Antoniadis, 2011), among others.

Although this list is not exhaustive, it underscores the breadth of approaches available for analysis. By combining these various methodologies, researchers aim to construct more precise and reliable models for machine condition monitoring. Through this integration, the potential for accurately identifying and predicting faults in machinery is significantly enhanced.

Machine learning-based condition monitoring of mechanical systems relies heavily on data. To amass a large dataset, it's essential to gather a vast array of data encompassing various degrees of faults and experimental conditions. Achieving this requires the creation of artificial faults through specific methods. Artificially injecting faults poses challenges, particularly when it comes to ensuring repeatability and control over the size of the fault. Traditional methods such as cutting tools or drill mills may lack accuracy, and be limited by the high hardness of the materials employed for bearings, in particular, when attempting to damage different parts of the bearing with varying fault sizes. Consequently, manually employing these tools often results in irregular fault sizes and dimensions. In contrast, laser injection offers a solution that provides repeatability and precise control over fault dimensions. By utilizing laser technology, faults can be consistently created even in very high strength material with accurate control over their size and shape, ensuring greater consistency and reliability in experimental conditions.

The rest of the paper is structured as follows. Section 2 provides insights into the experimental setup of the independent cart system, including the cart and bearing configuration. Following this, Section 3 elaborates on the setup involving picosecond laser technology. In Section 4, the paper delves into the specifics of the experimental campaign. Moving forward, Section 5 presents preliminary results derived from the conducted experiments. Finally, conclusions drawn from the study are discussed in Section 6.

2. Independent Cart System and Experimental Setup

The experimental setup for the independent cart system utilized in this study comprises eight straight motor modules, two curved modules, and a total of 12 carts. Each straight motor module features a 250-millimeter (mm) long stator, while the stator of the curved module measures 500 mm in length. Consequently, the combined length of the track defined by the 10 motor modules totals 3000 mm (see figure 1). With the system's capability to program each cart independently for a desired travel path, provided there are no collisions between carts, experiments were conducted with varying numbers of carts. Each cart, measuring 50 mm in length, consists of five pairs of permanent magnets and is equipped with a set of three rolling-element bearings as shown in figures 3 and 4. The two top bearings share identical geometry, with an external diameter of 25 mm, while the bottom bearing is slightly larger, with an external diameter of 35 mm. These bearings ensure secure attachment of the cart to the guide rail, which runs parallel to the linear motor modules (see figure 2). The motor modules are outfitted with coils that generate magnetic field patterns, enabling the system to achieve the desired trajectory and motion profile for each cart.

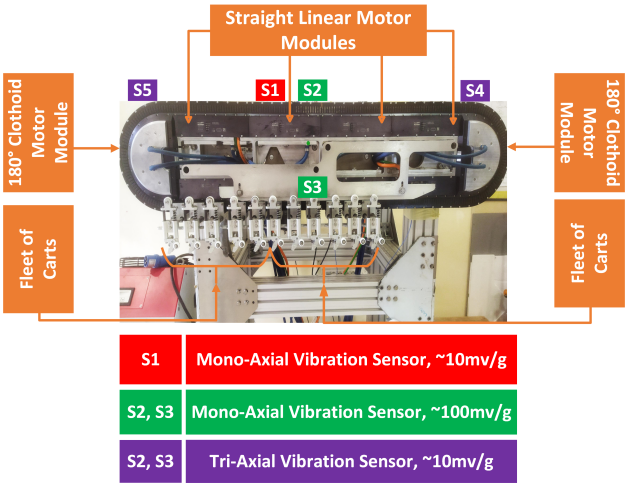

Figure 1. The independent cart system with Parallel guide rail.

To acquire vibration data, five vibration sensors were strategically installed at various locations throughout the system's geometry, as depicted in the figure 1. Among these sensors, three are monaxial, each with different sensitivities (e.g., 10mv/g and 100mv/g). The remaining two sensors are triaxial and are directly mounted onto the guide rail near the left and right sides of the system, with each axis exhibiting a sensitivity of approximately 10mv/g.

3. Picosecond Laser

An EKSPLA Atlantic 50 picosecond laser source was used to damage the bearings. It's a picosecond laser source which generates a Gaussian beam profile at the IR wavelength of 1064 nm. This kind of laser source produces ultrashort pulses in the picosecond regime thus allowing to ablate the inner (and the outer) race by creating a very precise in shape grooves without limitations in terms of hardness of the material to be harmed. The laser beam diameter in the focal position settled at $\phi \approx 10\ \mu$m, evaluated at $1/e^2$ intensity. A dedicated optical path for the IR wavelength allowed the laser beam exiting from its source to be delivered to the scanning head. This is a Raylase Supercan IV galvanometric scanner copuled with an 80 mm F-theta lens thus allowing a square working area with a side of 39 mm. The remaining movements, outside the above scan area, were instead guaranteed by the translation, in X and in Y- direction, of a stage on which the bearings to be damaged were placed. The translation of Z axis

Figure 2. The parallel guide rail.

allowed to damage the bearings by working at the correct focal height. The entire system set up in BrightLab laboratory of the DISMI Department is shown in Figure 5. Preliminary tests were conducted to evaluate the response of the material to the infrared radiation. These tests allowed us to correctly identify, and define, all the process parameters to be able to carry out damage with specific geometry, dimension and prescribed depth. The adopted laser parameters are summarized in Table 1.

Table 1. Laser parameters used during experiments.

Parameter	Unit of Measure	Value
Wavelength, λ	nm	1064
Average Output Power, P	W	13.32
Pulse Frequency, f	kHz	300
Pulse energy, E	µJ	44.4
Pulse duration, τ	ps	10
Pulse fluence, F	J/cm^2	56.56
Line spacing, s	µm	5
Marking speed, v_s	m/s	1
Number of passes on each groove, p		150

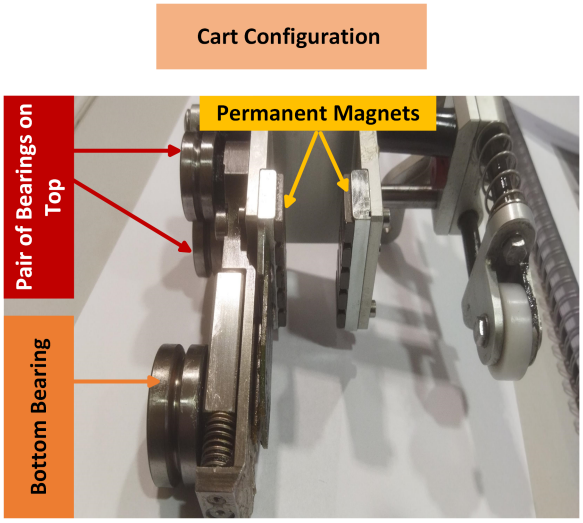

Figure 3. System's cart configuration.

4. Experimental Campaign

The experimental campaign can be divided into two main categories: fault injection and vibration data acquisition, with and without the presence of bearing faults. Fault injection campaigns, furthermore, can be categorized into two main types: those that do not involve dismantling the bearings and those that involve disassembled bearings. Initially, our approach aimed to create faults in bearings without the need for dismantling, utilizing Lab-available drill mill. However, due to the limited flexibility in maneuvering of the drill mill head caused by the close proximity of the bearing's inner and outer races, the faults injected were predominantly of an incipient nature. Consequently, these faults failed to fully encompass the entire grooves of the inner and outer races. Henceforth, these faults will be referred to as incipient fault types throught the remainder of this paper. Subsequently, we explored an alternative method using the EKSPLA Atlantic 50 picosecond laser to create faults in the bearings without disassembly. This approach allowed to reach controlled fault while entailing a challenging method to perform the damage of the bearing parts. The main difficulties were found in the creation of damage both in the inner race and in the outer race of the bearing and they referred to the following two aspects. The first is linked to the shielding effect of the laser radiation that some components of the non-disassembled bearing may have on the area that needs to be damaged. This inconvenience also occurred when specific supports were used to correctly orient (and strongly tilt) the bearing (e.g. the internal race didn't always allow the defect to be created in the external race in its entire axial extension due to the shielding effect performed). Instead, the second considered the need to create a groove with a predetermined depth on a strongly inclined component due to the considerations previously anticipated. To overcome these limitations, and also to be robust in ob-

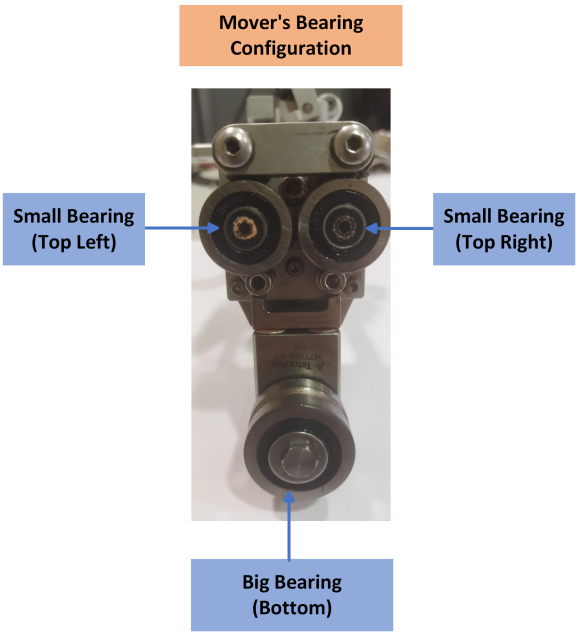

Figure 4. Cart's bearing configuration.

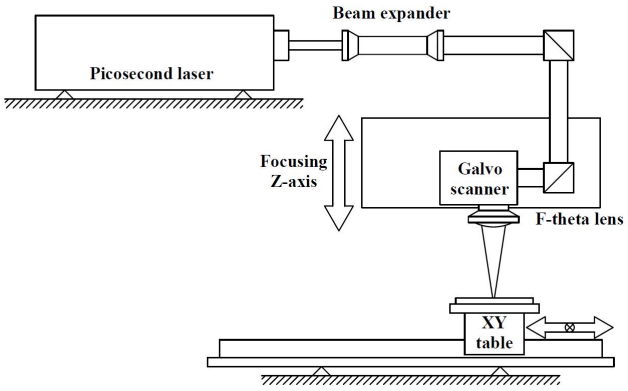

Figure 5. A schematic of the laser ablation system.

taining the damage on the various component of the bearings comparable to what was achieved on preliminary planar tests, an evaluation of the allowable depth of focus was required. In particular, by considering a beam quality factor M^2 of 1.5 and a laser beam diameter (evaluated at $1/e^2$ intensity) on the lens of $D_0 = 14$ mm, have been calculated:

- Rayleigh length z_f, as the distance from the beam waist where the beam radius is increased by a factor of the $\sqrt{2}$:

$$z_f = \frac{\pi \left(\frac{D_0}{2}\right)^2}{M^2 \lambda} \approx 100\ \mu m \tag{1}$$

- Depth of Field (D.O.F.), as the distance either side of the beam waist, D_0, over which the beam diameter grows by 5%

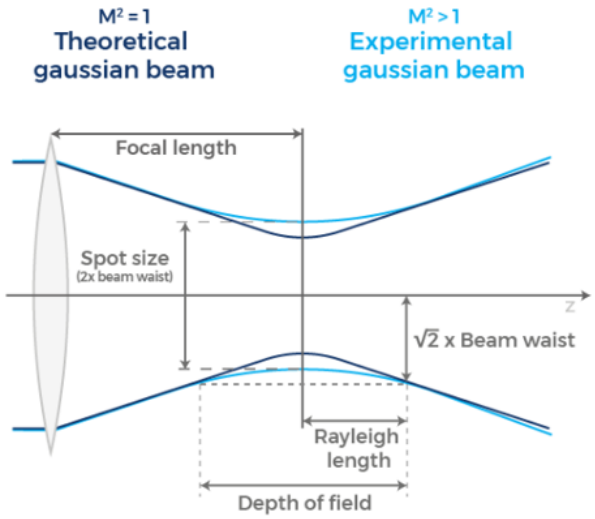

Figure 6. Pico-second laser beam profile

$$\text{D.O.F.} = \pm 0.08 \pi D_0^2 M^2 \lambda \approx 118\ \mu m \tag{2}$$

The modest value of the depth of Field (D.O.F.), which settles at 118 μm for our laser, did not allow for damaging the bearing components in a single laser pass. Therefore, a multi-pass approach was needed. This methodology involves focusing the laser beam on a target zone of the component that needs to be damaged. The process carried out is characterized by reaching the prescribed depth in the area where the laser was focused, and by unworked areas where the laser was unable to completely deposit its energy and properly ablate the material. The processing area can therefore be limited to a rectangle having as its height the depth of field previously calculated. The areas not included within this height will instead remain untreated due to the unfocused conditions. An incremental increase in depth is needed and allowed by varying the height of the galvanometric head (and correspondingly recovering the *X* position by advancing with the *XY* table). In this way, by focusing on a lower area, further ablation processing is possible. The process is performed continuously until the intended damage shape is achieved. The reached depth had a tolerance of ± 0.15 mm from the nominal shape. Finally, to fully overcome the limitations related to the first issue explained above, the bearings were completely dismantled. This way, individual parts of the bearing were fully exposed, facilitating controlled fault injection. The damage process was unaffected by the presence of, for instance, balls between the inner and outer races, which obscured the area to be damaged. Thus, better and more precise flat-bottom grooves were created using the multi-pass criteria mentioned above. An optical microscope (Mod. Nikon LV100ND), was used to characterize the final shape of the fault in terms of dimensions and, by changing the depth of focus.

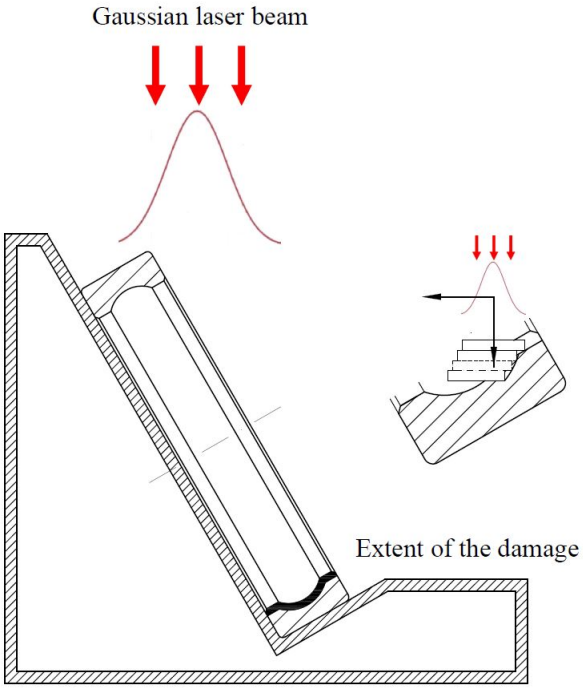

Figure 7. Positioning of bearings on an ad-hoc support. The operating principle of the multi-altitude approach for progressive focusing is explained in the enlarged image.

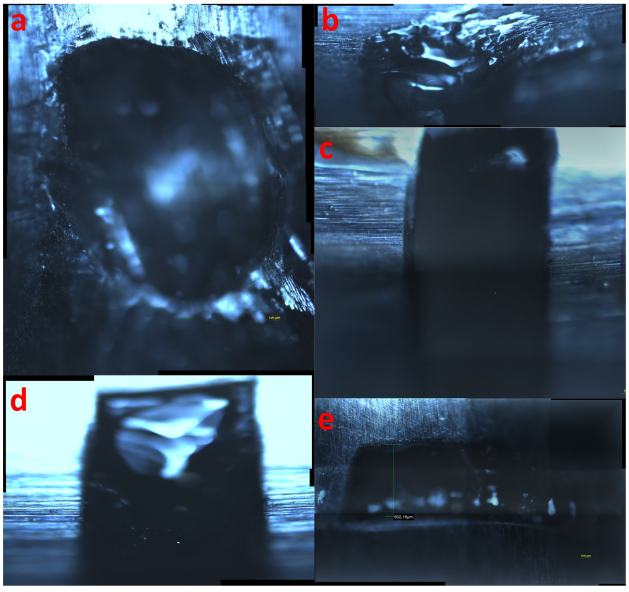

Figure 8. Microscopic view of bearing faults: a) Incipient version IR fault of bottom bearing, b) Incipient version OR fault of bottom bearing, c) Lase version 0.5 OR fault of top bearing, d) Lase version 1.0 OR fault of bottom bearing, e) Lase version 0.5 IR fault of bottom bearing.

Table 2. Bearing type, fault type, and fault version.

Bearing Type	Fault Type	Fault Version			
		Incipient Width	Laser 0.5 Width	Laser 1.0 Width	Laser 2.0 Width
Top Bearing	OR	NA	0.5	1.0	2.0
	IR	0.75	0.5	1.0	2.0
	BF	NA	0.5	1.0	2.0
	OROS	NA	0.5	NA	NA
Bottom Bearing	OR	1.3	0.5	1.0	2.0
	IR	1.4	0.5	1.0	2.0
	BF	NA	0.5	1.0	NA
	OROS	NA	0.5	NA	NA

The microscopic view of the some of the faults created without dismantling the bearings is illustrated in the figure 8. It is evident that the depth of the faults varies non-uniformly due to the challenges mentioned earlier. A tabular summary of the fault injection campaign without dismantling the bearings is presented in the table 2. In the table, ”IR” represents inner race faults, ”OR” denotes outer race faults, ”BF” signifies ball/roller faults, and ”OROS” indicates outer race outer surface faults. Whereas, laser versions 0.5, 1.0, and 2.0 represent the nominal width (in mm) of the injected faults.

5. Results

The experiments involved varying the number of movers and different experiment types, each focusing on different areas of the system, such as the straight path on the top or bottom side, or the curved side, with varying numbers of movers. However, the results presented are specifically for a particular experiment type involving a single mover traversing the straight path on the top side of the system, demonstrating back-and-forth motion. This experiment was conducted at different speeds: 1000 mm/s, 2000 mm/s, and 3000 mm/s. It is important to note that the results will not be discussed in terms of fault identification based on fault frequency. Instead, the focus will be on highlighting differences in the vibration data concerning fault injection types and fault sizes.

The figure 9 illustrates the Fast Fourier Transform (FFT) of the data obtained during the experiment conducted at a speed of 1000mm/s, showcasing different versions of IR faults in the top bearing. In the legend, ”F” indicates the presence of a fault, while ”H” denotes healthy conditions. Additionally, ”S1000” represents the linear speed of the cart. ”V” signifies the laser version of fault injection, while ”Incipient Fault” denotes manual fault injection. It is important to note that only one of the top couple of bearings is faulty at a time. Moreover, the width of the impulses in the data with faulty conditions appears to be directly correlated with the size of the faults; sharper faults result in narrower impulse widths. The same behavior is observed in the case of the outer race fault of the bottom bearing, as illustrated in the figure 12.

As evident from the table 2, the Incipient type IR fault in the top bearing measures 0.65mm, which closely aligns with the laser version 0.5 fault. This similarity is also reflected

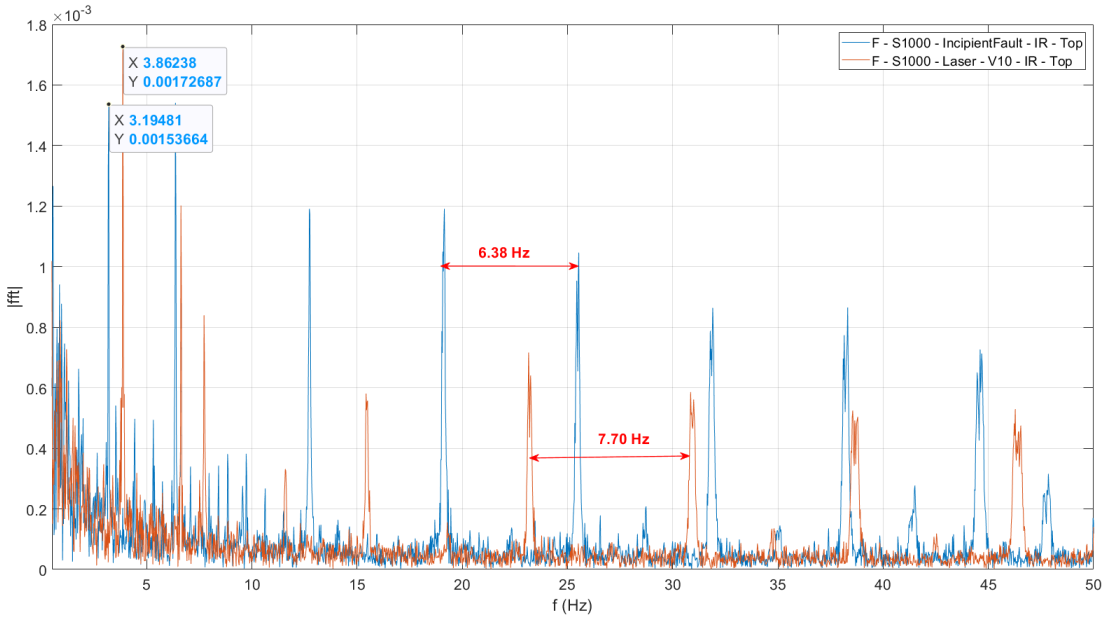

Figure 9. The FFT of the vibration data with an incipient and laser version 1.0 type inner race fault in the top bearing, at a linear speed of 1000 mm/s.

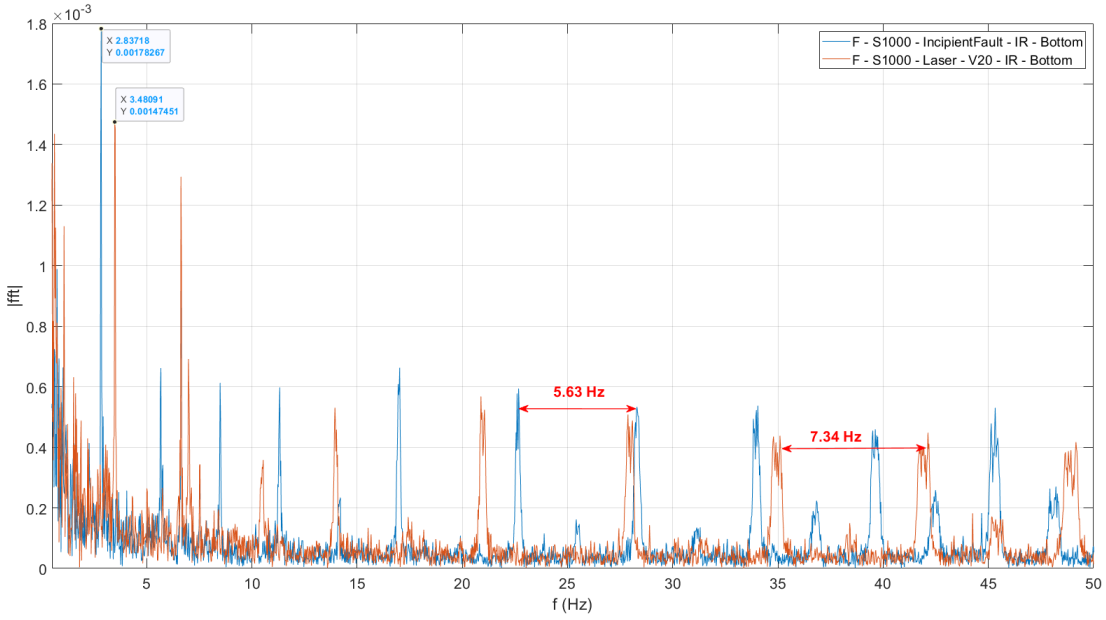

Figure 10. The FFT of the vibration data with an incipient and laser version 2.0 type inner race fault in the bottom bearing, at a linear speed of 1000 mm/s.

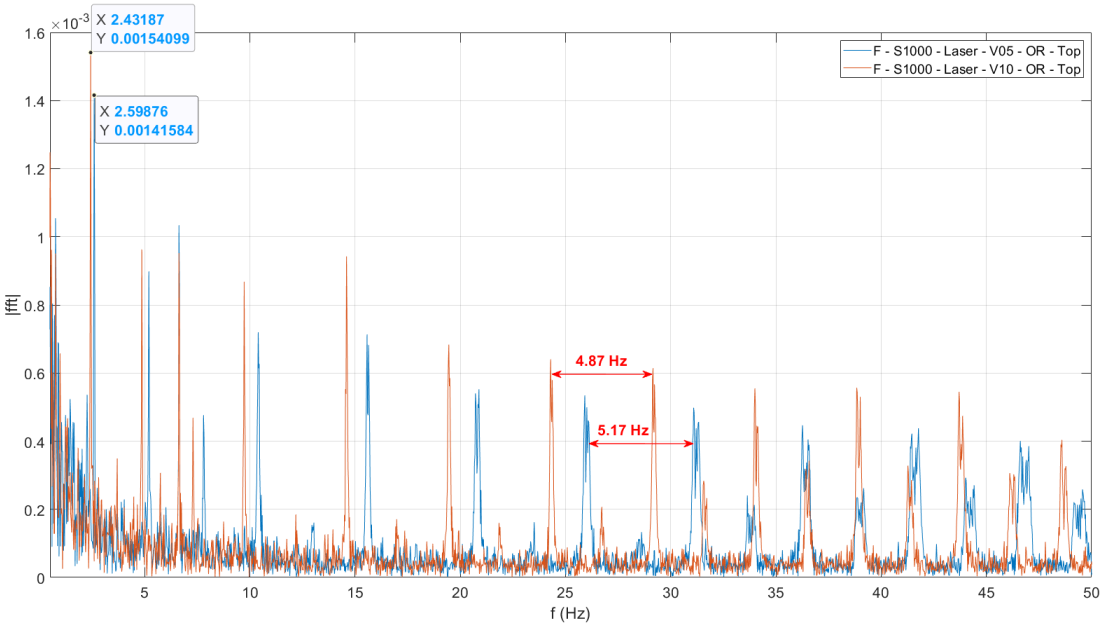

Figure 11. The FFT of the vibration data with laser version 0.5 and laser version 1.0 type outer race faults in the top bearing, at a linear speed of 1000 mm/s.

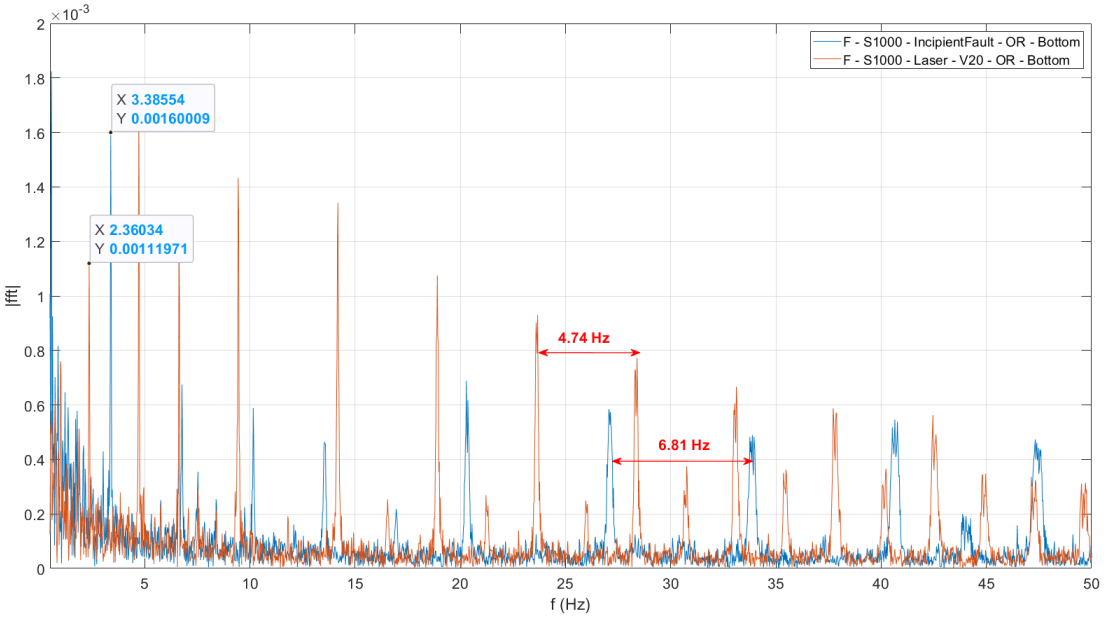

Figure 12. The FFT of the vibration data with an incipient and laser version 2.0 type outer race fault in the bottom bearing, at a linear speed of 1000 mm/s.

in the width of the impulses in the FFT of the vibration signal. However, it's noteworthy that the width of the incipient fault is not uniform throughout the fault area, nor does it completely cover the groove of the inner race where the rolling element glides. Therefore, a detailed explanation and analysis of these differences are yet to be conducted. Similarly, in the case of the IR bottom bearing fault, the incipient fault, approximately 1.4 mm wide at its widest, shows FFT characteristics more akin to the laser version 2.0 fault type as depicted in figure 10. Notably, for the incipient type IR fault of the bottom bearing, the modulating frequency appears to be 2.83 Hz, with even harmonics exhibiting higher energy than the odd harmonics. Conversely, for the laser version 2.0 fault in the bottom bearing, the modulating frequency seems to be 3.48 Hz, with even harmonics having more energy than the odd harmonics.

Likewise, for the IR top bearing fault in figure 9, the incipient type fault measuring approximately 0.75mm exhibits FFT characteristics more similar to the laser version 1.0 fault type. Interestingly, for the incipient type IR fault of the top bearing, the modulating frequency appears to be 3.19 Hz, with even harmonics having higher energy than the odd harmonics. Conversely, for the laser version 1.0 IR fault in the top bearing, the modulating frequency seems to be 3.86 Hz, with even harmonics exhibiting more energy than the odd harmonics.

Regarding the OR bottom bearing fault, the incipient fault, approximately 1.3 mm wide at its widest, exhibits FFT characteristics more aligned with the laser version 2.0 fault type as shown in figure 12. Notably, for the incipient type OR fault of the bottom bearing, the modulating frequency appears to be 3.38 Hz, with even harmonics demonstrating higher energy than the odd harmonics. Conversely, for the laser version 2.0 fault in the bottom bearing, the modulating frequency seems to be 2.36 Hz, with even harmonics having more energy than the odd harmonics.

Lastly, in the case of the OR top bearing fault in figure 11, the FFT of the laser version 0.5mm resembles more closely the laser version 1.0 fault type. Interestingly, for the version 0.5 OR fault of the top bearing, the modulating frequency appears to be 2.59 Hz, with even harmonics demonstrating higher energy than the odd harmonics. Conversely, for the laser version 1.0 fault in the top bearing, the modulating frequency seems to be 2.43 Hz, with even harmonics exhibiting more energy than the odd harmonics.

6. Conclusion

In order for the dataset to be utilized in developing new algorithms, it is imperative that at least a subset of the data exhibits clear fault signatures. The laser method of fault injection offers precise control over fault dimensions, ensuring repeatability. The data acquired from this experimental campaign could serve as a benchmark for the development and testing of condition monitoring algorithms, whether they are machine learning-based, statistically based, or employ classical signal processing techniques.

Acknowledgment

Authors gratefully acknowledge the European Commission for its support of the Marie Sklodowska Curie Program through the H2020 ETN MOIRA project (GA 955681).

References

Bearing data center, case western reserve university (cwru). (n.d.). Retrieved from {http://csegroups.case.edu/bearingdatacenter/hom.}

Cavalaglio Camargo Molano, J., Capelli, L., Rubini, R., Borghi, D., & Cocconcelli, M. (1968). Determination of threshold failure levels of semiconductor diodes and transistors due to pulse voltages. *IEEE Transactions on Nuclear Science*, *15*(6), 244-259.

Cheng, K., RC.and Chen. (2022). Ball bearing multiple failure diagnosis using feature-selected autoencoder model. *Int J Adv Manuf Technol 120, 4803–4819 (2022). https://doi.org/10.1007/s00170-022-09054-x*(120), 4803–4819.

Cheng, R.-C., Chen, K.-S., Liu, Y., Chang, L.-K., & Tsai, M. C. (2021). Development of autoencoder-based status diagnosis method for ball bearing tribology status monitoring. *The Proceedings of The 9th IIAE International Conference on Industrial Application Engineering 2020.* Retrieved from https://api.semanticscholar.org/CorpusID:236644837

Fan, Y., Zhang, C., Xue, Y., Wang, J., & Gu, F. (2020). A bearing fault diagnosis using a support vector machine optimised by the self-regulating particle swarm. *Shock and Vibration*. Retrieved from https://api.semanticscholar.org/CorpusID:214661891

Fan, Z., Wang, Y., Meng, L., Zhang, G., Qin, Y., & Tang, B. (2023). Unsupervised anomaly detection method for bearing based on vae-gan and time-series data correlation enhancement (june 2023). *IEEE Sensors Journal*, *23*(23), 29345-29356. doi: 10.1109/JSEN.2023.3326335

Hu, B. (2023). *bearing dataset.* IEEE Dataport. Retrieved from https://dx.doi.org/10.21227/5p7e-pz02 doi: 10.21227/5p7e-pz02

Hu, Y., Wei, R., Yang, Y., Li, X., Huang, Z., Liu, C., Y.and He, & Lu, H. (2022). Performance degradation prediction using lstm with optimized parameters. *Sensors 2022, 22, 2407. https://doi.org/10.3390/s22062407*, *2407*(22).

Jabbar, A., Cocconcelli, M., D'Elia, G., & Strozzi, R., M.and Rubini. (2023). Results on experimental data analysis of independent cart systems in non-stationary conditions. In *Surveillance, vibrations, shock and noise, institut supérieur de l'aéronautique et de l'espace [isae-supaero], jul 2023, toulouse, france.*

Jabbar, A., D'Elia, G., & Cocconcelli, M. (2023). Experimental setup for non-stationary condition monitoring of independent cart systems. In *In: Kumar, u., karim, r., galar, d. and kour, r. (eds). international congress and workshop on industrial ai and emaintenance 2023. iai 2023. lecture notes in mechanical engineering.*

Lee, J., Qiu, H., Yu, G., & Lin, J. (2007). *Rexnord technical services, ims, university of cincinnati. "bearing data set", nasa ames prognostics data repository, nasa ames research center, moffett field, ca.* Retrieved from {http://ti.arc.nasa.gov/tech/dash/pcoe/prognostic-data-repository/.}

Sun, B., & Liu, X. (2023). Significance support vector machine for high-speed train bearing fault diagnosis. *IEEE Sensors Journal*, *23*(5), 4638-4646. doi: 10.1109/JSEN.2021.3136675

Walther, S., & Fuerst, A. (2022). Reduced data volumes through hybrid machine learning compared to conventional machine learning demonstrated on bearing fault classification. *Appl. Sci. 2022, 12, 2287. https://doi.org/10.3390/app12052287*, *2287*(12).

Wan, S., Liu, J., Li, X., Zhang, Y., Yan, K., & Hong, J. (2022). Transfer-learning-based bearing fault diagnosis between different machines: A multi-level adaptation network based on layered decoding and attention mechanism. *Measurement*, *203*, 111996. Retrieved from https://www.sciencedirect.com/science/article/pii/S0263224122011927 doi: https://doi.org/10.1016/j.measurement.2022.111996

Yiakopoulos, C., Gryllias, K., & Antoniadis, I. (2011). Rolling element bearing fault detection in industrial environments based on a k-means clustering approach. *Expert Systems with Applications*, *38*(3), 2888-2911. Retrieved from https://www.sciencedirect.com/science/article/pii/S0957417410008791 doi: https://doi.org/10.1016/j.eswa.2010.08.083